Effects of reactive oxidants generation and capacitance on photoelectrochemical water disinfection with self-doped titanium dioxide nanotube arrays

Kangwoo Cho[a],*, Seonggeun Lee[b], Hyeonjeong Kim[a], Hyung-Eun Kim[b], Aseom Son[b], Eun-ju Kim[b], Mengkai Li[c], Zhimin Qiang[c], Seok Won Hong[b],*

[a] Division of Environmental Science and Engineering, Pohang University of Science and Technology (POSTECH), Pohang 790-784, Republic of Korea
[b] Water Cycle Research Center, Korea Institute of Science and Technology (KIST), Hwarangro 14 gil, Seongbuk-gu, Seoul, 02792, Republic of Korea
[c] Key Laboratory of Drinking Water Science and Technology, Research Center for Eco-Environmental Sciences (RCEES), University of Chinese Academy of Sciences, Chinese Academy of Sciences, 18 Shuang-qing Road, Beijing 100085, China

ARTICLE INFO

ABSTRACT

We herein provide photoelectrochemical (PEC) disinfection activities of anodically prepared TiO$_2$ nanotube (TNT) arrays (diameter ˜ 100 nm, length ˜ 16 μm on average) that were electrochemically self-doped before (bk-TNT) and after (bl-TNT) an atmospheric annealing at 450 °C. The X-ray diffraction indicated predominating anatase TiO$_2$ signal on bl-TNT, while substantial lattice distortion was noticed for bk-TNT. Although the X-ray photoelectron spectra indicated negligible Ti^{3+} on surface of both TNTs, linear sweep (cyclic) voltammetry and electrochemical impedance spectrometry confirmed the bk-TNT to show greater double layer capacitance and overall photocurrent, coupled with lower charge transfer resistance. Nevertheless, the PEC disinfection of *E. coli* was significantly invigorated on bl-TNT, while the bactericidal rates in tap water were comparable or even far greater than those in 0.1 M Na$_2$SO$_4$ solutions, depending on [*E. coli*]$_0$ (10^5 or 10^7 CFU/mL). Under a presumed diffusion-controlled kinetic regime in this study, observed effects of capacitance and electrolyte could be interpreted in terms of electrostatic interaction between the electrical double layer of photoanodes and charged bio-solids, such as repulsion by co-ions (SO$_4^{2-}$) and adsorption/surface blocking. Analogous PEC experiments on model organic compounds degradation (4-chlorophenol and methylene blue) corroborated a long-term stability of the bl-TNT (up to 30 consecutive cycles) and the role of surface hydroxyl radical as the primary oxidant.

1. Introduction

Semiconductor photocatalysts pave potential ways for environmental remediation and green energy conversion, in complementary with existing biological and chemical processes. The reactive oxygen species (ROS) as the reaction intermediates (such as ˙OH, H$_2$O$_2$, O$_2^-$˙) together with direct transfer of charge carriers (electron and hole) to substrates (pollutants and water) account for the dual functions of the photocatalytic redox reactions, in order to decompose organic/inorganic pollutants (including pathogens) for water/air purification coupled with conversion of solar energy into electricity and/or chemical energy carriers [1]. A serious body of research has been given to titanium dioxide (TiO$_2$), utilizing the valence band holes and conduction band electrons with proper electrochemical potentials for the environmental applications [2,3]. TiO$_2$ is robust, inexpensive, and

environmentally benign material, for implementations in photoelectrochemical (PEC) systems.

The primary research focus on photocatalysts has been given to the engineering of band positions and/or surface defects for elevation of light absorbance and competing with the charge recombination among many other purposes [1]. The separation of photo-generated electron/hole pair could be enhanced by surface modification (*e.g.*, defect formation and hetero-atom doping), where co-catalysts trapping the charge carriers facilitate the charge migration for surface reactions [3]. Doping of external elements could reduce the bandgap by introducing additional energy levels in forbidden band gap, although these also act as charge carrier recombination center. For TiO$_2$ photocatalysts, an enrichment of Ti^{3+} species or self-doping on surface has been reasoned to improve the electronic and optical properties [4]. Descending from reports on hydrogenated black colored TiO$_2$ with surface disorder by

proton intercalation [5,6], partial reduction of TiO_2 has been interrogated *via* reactions with chemical reagents (*e.g.*, H_2 gas, hydrazine) often in the presence of catalysts (*e.g.*, Pd) and high energy input (*e.g.*, Ar^+, laser bombardment) [4]. Cathodic polarization has been evinced to be a plausible way for the self-doping of TiO_2 in mild conditions (room temperature and atmospheric pressure) to minimize costly and hazardous fabrication procedures [7]. TiO_2 nanotube (TNT) array has been predominantly employed for the cathodization to allow propagation of surface states and charge transfer to the current collector [8–10]. Combined improvements in physicochemical properties were reported in electrical conductivity, charge transfer resistance, light absorptivity, and capacitance among others [10,11], which have been utilized for photochemical (PC) water splitting [12] and pollutants degradation [13], electrochemical (EC) oxidants generation [8,14], and supercapacitor [15,16]. A recent report further corroborated that the benefits of electrochemically self-doped TNT could be intensified in PEC system for aqueous pollutants degradation and H_2 generation [17].

The morphology/crystallinity of TNT, electrolyte, and cathodization conditions (potential bias, duration) would affect the level of oxygen vacancy (O_v) formation and/or proton intercalation, whose effects on aqueous pollutants abatement are not fully understood, especially in PEC configurations. To this end, the aim of this study comparatively evaluated cathodically self-doped TNT arrays with variable levels and distributions of the self-dopants for PEC water treatment, with primary focus on the disinfection efficacy. The most feasible application of TiO_2 material to water treatment would currently include disinfection of potable water [18], considering light penetration and pollutants load. This study revealed that, under a diffusion limited reaction regime, the capacitance rather than the reactive oxidants generation primarily determines the antibacterial (*E. coli*) activity, which should be an important consideration for engineering of PEC water disinfection processes.

2. Experimental

2.1. Materials

Ti foil and Pt coil were obtained from Alfa Aesar with purities greater than 99.5% in metal base. The metal samples were sonicated in diluted acetone for 0.5 h prior to usage. Ethylene glycol and NH_4F were purchased in the purity of 99% (Showa Chemical Industry). Methylene blue (MB), Na_2SO_4, KH_2PO_4, NaOH, *tert*-buthanol (TBA), methanol (ME), 4-chlorophenol (4-CP), *p*-nitrosodimethylaniline (RNO), and H_2O_2 were obtained from Sigma Aldrich in reagent grade.

2.2. Fabrication of the self-doped TNT array

Ti foil with working area of $9.5\,cm^2$ in parallel with a Pt coil (average distance: 1 cm) was anodized in ethylene glycol containing H_2O (2.5 wt%) and NH_4F (0.2 wt%) for 5 h under a constant potential (45 V), using a DC power supply (TDP-1005b, Toyotech), at controlled temperature (25 °C). The anodized samples were subject to annealing either at 200 or 450 °C for 1 h to produce red-brown or white colored TiO_2, respectively. Subsequently, cathodic self-doping was carried out in a two electrodes configuration connected to a potentiostat (SP-150, Biologic), under constant current (160 mA) for 90 s employing the Pt coil as the counter electrode. For the cathodization processes, 0.1 M phosphate buffer (pH 7.2, adjusted by NaOH) was used as the electrolyte. The samples annealed at 450 °C before the self-doping showed blue color. The other samples pre-annealed at 200 °C underwent additional annealing at 450 °C in N_2 atmosphere after the cathodization, to produce black colored array. The apparent electrochromism allowed to label the two sets of samples as blue (bl-TNT) and black TNT (bk-TNT) array, respectively, in accordance to literature.

Scanning electron microscopy (SEM, Inspect F50, FEI) was employed in order to observe morphology of the synthesized TNT array at multiple magnification ratios. Electron Dispersive X-ray Spectroscopy (EDS) estimated elemental composition. X-ray Diffraction (XRD, X'Pert PRO, PANalytical) analysis was performed to assess the crystalline structure with Cu Ka radiation (40 kV, 40 mA). X-ray Photoelectron Spectroscopy (XPS, PHI 5000 VersaProbe, Ulvac-PHI) determined the surface oxidation states using monochromator Al Ka (1486.6 eV) anode.

2.3. Characterization of photoelectrochemical properties

In order to examine the photoelectrochemical properties of bl- and bk-TNT, linear sweep voltammetry (LSV) and cyclic voltammetry (CV) were performed in a three-electrode configuration in quartz cells (working volume: 40 mL), employing Pt coil and Ag/AgCl/saturated KCl (BASi) as counter and reference electrode, respectively. The distance between the anode and cathode was fixed at 1 cm, while the tip of reference electrode was positioned close to the anode. Electrochemical impedance spectroscopy (EIS) analysis was performed under the open circuit potential between scan frequency of 100 kHz to 10 mHz and with a 10 mV rms sinusoidal modulation. The series of analysis were performed in 0.1 M Na_2SO_4 solutions at scan rates from 1 to 50 mV s^{-1} in dark and UV irradiation conditions. For the UV irradiation to the reactor, a custom-made black box was utilized to install six 4 W black light UVA lamps (F4T5, Sankyo Denki). The peak wavelength from the light sources was 352 nm and the total incident light intensity determined by an optical power meter (Newport 1918-R) was 2.5 mW/cm^2.

2.4. Photoelectrochemical disinfection and organic substrates degradation experiments

Photo-electrochemical experiments for disinfection and organic compounds degradation were performed, using the three electrodes configuration described above, in PC (UV irradiation only), EC (potential bias only), and PEC (PC + EC) conditions. The external potential bias was set at 1 V versus the reference electrode. The initial bacterial and viral densities (N_0) of the model pathogens (*E. coli* and MS2 coliphage) were either 10^5 or 10^7 CFU/mL (or PFU/mL), whereas the initial concentration (C_0) of organic compounds (MB, 4-CP, and RNO) was fixed at 10 or 20 µM. Before all experiments, the reactor was rested for 20 min in dark to evaluate the adsorptive removal of the coliforms/pollutants. Small aliquot of samples was periodically collected and serially diluted to a certain concentration for further analysis.

2.5. Analysis

Bulk pH and conductivity were measured with a pH meter (Mettler Toledo) and a portable conductivity meter (VWR International). The free chlorine concentration was estimated with DPD (*N,N*-diethyl-*p*-phenylenediamine) reagent (Hach), based on the absorbance at 530 nm in UV-VIS spectrophotometer (S-3100, Scinco). The [MB] was determined based on the absorbance at 664 nm, whereas [4-CP] and [total organic carbon (TOC)] were measured by a high performance liquid chromatography (HPLC, 1260 infinity Quaternary LC VL, Agilent) and TOC analyzer (TOC-L CPH, Shimadzu). The primary oxidants generated from the self-doped TNT arrays were determined based on electron paramagnetic resonance (EPR) spectra during PEC treatment of 0.1 M Na_2SO_4 solutions containing 5,5-dimethyl-pyrroline N-oxide (DMPO) as a spin-trapping agent. The EPR spectra were recorded by a JES-TE 300 spectrometer (JEOL, Japan) under the following specific conditions; microwave power = 1 mW, microwave frequency = 9.418 GHz, center field = 3351 G, modulation width = 0.2 mT, and modulation frequency = 100 kHz.

E. coli (ATCC 8739) and MS2 coliphage (ATCC 15597-B1) were selected for bactericidal and virucidal activity test. *E. coli* stock was incubated in 30 mL of nutrient broth at 37 °C for 18–24 h. The samples were washed with phosphate-buffered saline (pH 7.2) and harvested by
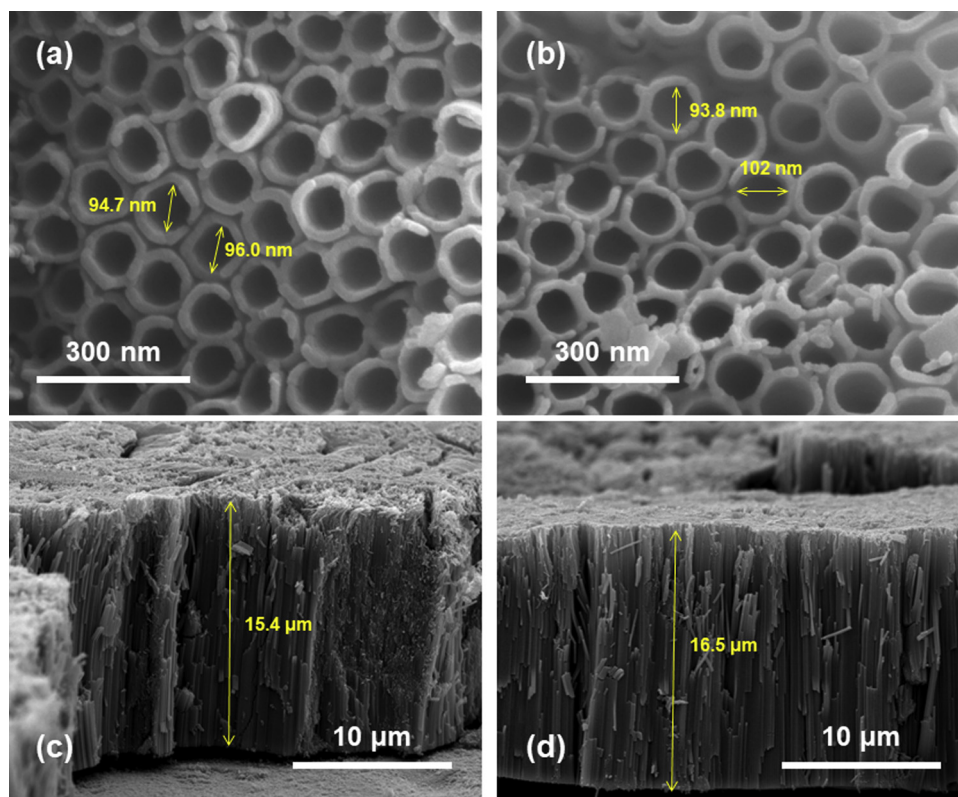
Fig. 1. Horizontal and vertical SEM images for (a, c) bl-TNT and (b, d) bk-TNT arrays.
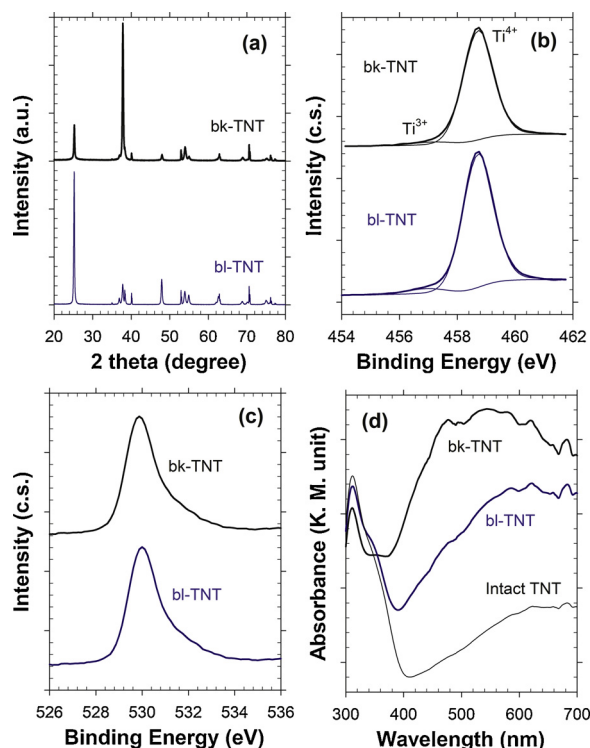

Fig. 2. Physico-chemical properties of bl- and bk-TNT arrays based on (a) XRD signals, XPS intensities for (b) Ti 2p and (c) O 1s, together with (d) light absorbance in DRS.

centrifugation at 3000 rpm for 15 min (repeated 3 times). The obtained *E. coli* cells were re-suspended in 20 mL of the phosphate-buffered saline and refrigerated before use. MS2 coliphage stock was prepared

with *E. coli* C3000 (ATCC 15597) as a host. The *E. coli* host was cultivated in a medium containing 0.001% thiamine, 0.01% glucose, 0.1% yeast extract, 0.8% NaCl, 1% tryptone, and 2 mM CaCl$_2$. MS2 coliphage was inoculated and incubated to the cultured host *E. coli* for 18–24 h at 37 °C. After incubation, the solution was centrifuged at 3000 rpm for 15 min, and the supernatant was filtered through 0.22 μm syringe filter. The spread plate method was employed to determine the population of *E. coli*, while the population of MS2 coliphage was determined by double-layer plaque assay method.

3. Results

3.1. Physico-chemical properties

Fig. 1 presents the horizontal and vertical SEM images of the TNT arrays electrochemically self-doped before (bk-TNT) and after (bl-TNT) the atmospheric annealing step at 450 °C. During the anodization of Ti foil, an electric-field assisted oxidation of Ti and F$^-$ accelerated chemical etching would occur in parallel [19]. A multi-porous layer structure was observed, on account of the resulting dissolution of Ti in the form of TiF$_6^{2-}$ [20,21]. The bl- and bk-TNT were characterized by similar diameter of 94–102 nm and length of 15.4–16.5 μm. The morphology of TNT is known to be affected primarily by the anodic bias during synthesis and partly by electrolyte composition [19], whereas the cathodization processes showed marginal influence on the topography [10,13]. An excessive current density and H$_2$ bubble formation during the cathodization were noted to damage the array structure [22]. The EDX analysis estimated O/Ti atomic ratio for the bl- and bk-TNT to be 1.6 and 1.5, where the observed sub-stoichiometry (*i.e.*, O/Ti < 2) might roughly indicate oxygen deficiency induced by self-doping.

The XRD diffractograms shown in Fig. 2a were in general agreement with anatase TiO$_2$ for both samples [14], in terms of superimposable location of the peaks. However, the most intense signal was observed

from (101) for bl-TNT but (004) for bk-TNT, indicating a substantial lattice distortion for the bk-TNT. The X-ray photoelectron spectra could locate the strong Ti 2p peak at binding energy of 458.7 (Fig. 2b), exclusively from Ti^{4+} for both arrays. Further deconvolution of the peaks indicated negligible contribution from Ti^{3+} on surface, while the XPS signals for O 1s were also superimposable for bl- and bk-TNT. Evidences have been presented that the cathodic self-doping of TNT initiates from the bottom of nanotube structure and proceeds outwards along the wall [23,24]. Thus, depending on the tube length and passed charge during cathodization, the self-dopants could be localized near the bottom of tubes not to be detected by surface limited analysis (XPS).

DRS spectra shown in Fig. 2d indicate virtually comparable UV absorbance from 310 to 350 nm (UVA), whereas substantial increases in visible light absorptivity were noted by self-doping along with the formation of mid-gap states [9]. In particular, Ti^{3+} and O vacancy were estimated to have energy levels at 0.3–0.8 eV and 0.7 eV below the conduction band edge, respectively [25]. Minute absorbance of visible light was noted even for the intact TNT, possibly due to an imperfect formation of anatase during annealing, particularly inside the nanotubes (*e.g.*, bottom). In agreement with the observed electrochromism, the maximum light absorbance of bl-TNT was noted at wavelengths exceeding 570 nm, whereas intense absorbance occurred in shorter wavelength range for the bk-TNT. These observations implied higher levels of donor density and bandgap narrowing for bk-TNT [10]. An augmented level of doping could broaden the mid-gap state continuum, even merging either with conduction or balance band [5].

3.2. Electrochemical properties

Fig. 3 illustrates the voltammetry behaviors of self-doped TNT arrays in terms of LSV, CV, and EIS in Na_2SO_4 solutions. The capacitive current of bk-TNT (in dark) was found to be far greater than bl-TNT (Fig. 3a) in the potential window without the water splitting [10,14]. The mean dark current density almost linearly increased with the scan rate from 1 to 50 mV s^{-1} (Fig. S1), which confirmed the electrical double layer capacitor behaviors of the self-doped TNT arrays [14] in this potential scan range (0.5–1.2 V NHE). However, the elevation in current value under illumination, which would be associated with oxygen evolution reaction (OER), was more pronounced for the bl-TNT. Considering the comparable UV absorbance at 352 nm (Fig. 2d), recombination to the mid-gap states was presumed to be greater for bk-TNT, leading to net lower Faradaic photocurrent. TiO_2 is a n-type semiconductor and intrinsically shows marginal current wave upon an increasing anodic potential bias, due to the depletion of the majority carrier (electron) at the interface [3]. Therefore, the rate of surface oxidants (OER intermediates) formation could have a minor dependency on the anodic bias, when the interfacial charge transfer is rate-limiting under a Zener limit. On the other hand, the onset of anodic wave from OER appeared earlier for bk-TNT (˜2 V Ag/AgCl, Fig. 3b) than for bl-TNT (˜ 2.5 V Ag/AgCl), as reported previously [10], indicating that charge transfer mediation by surface states (self-dopants) would decrease the OER overpotential [3]. In parallel, formations of O_v along with the partial reduction of Ti^{4+} to Ti^{3+} would shift the enthalpy change for the higher oxide formation, a principal determinant of OER activity [26]. On the other hand, the Nyquist plot (Fig. 3c) suggested by far lower charge transfer resistance (R_{ct}) for OER on bk-TNT in dark, based on the intercepts of projected semicircles on Z_{re} axis. However, the R_{ct} of bl-TNT was observed to decrease significantly upon the UVA irradiation, to be virtually similar with that of bk-TNT. Whether or not being illuminated, bl-TNT showed more complete semicircles under identical frequency range, corroborating substantially smaller double layer capacitance [17].

3.3. Photoelectrochemical disinfection

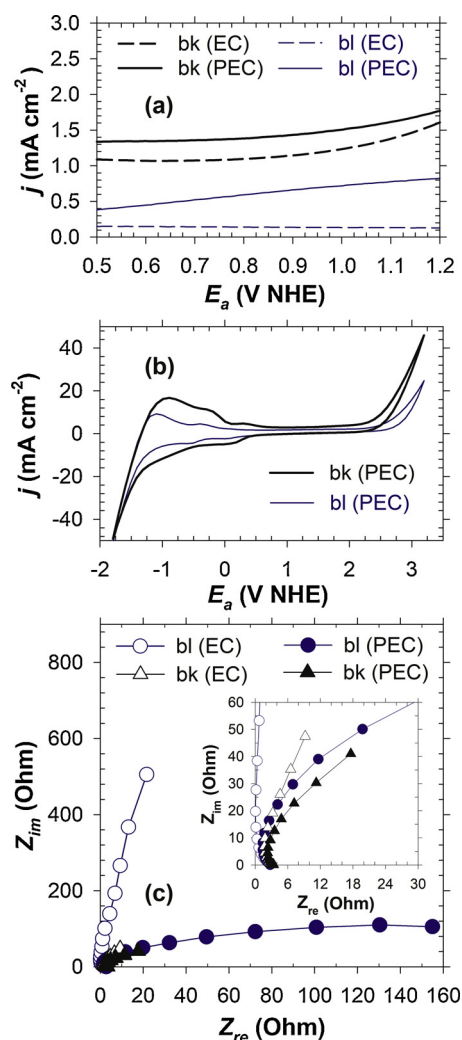The disinfection activities of TNT arrays were evaluated under

Fig. 3. Photo-electrochemical properties of bl- and bk-TNT arrays based on (a) LSV, (b) CV, and (c) Nyquist plot (Electrolyte = 0.1 M Na_2SO_4; Scan rate = 50 mV s^{-1} for LSV/CV; scan frequency =100 kHz - 10 mHz with 10 mV rms sinusoidal modulation versus open circuit potential for EIS).

variable energy input scenarios in 0.1 M Na_2SO_4 solutions (conductivity: 2.2 mS cm^{-1}), and in tap water (0.21 mS cm^{-1}) aiming at potential applications for point-of-use disinfection. Fig. 4a–c comparatively illustrate the logarithmic inactivation efficiency of *E. coli* (initial concentration of 10^5 CFU mL^{-1}) during 10 min of reaction. The mean log removal was less than 0.1 by photolytic disinfection under the UVA irradiation without TNT, on account of relatively low light intensity of the employed lamps (total 24 W). The bactericidal reaction was also sluggish at the anodic bias of 1 V Ag/AgCl in dark, despite a slight enhancement on bk-TNT. It has been known that a practically reliable EC water treatment (including disinfection) would require an anodic potential greater than 2 V NHE [27,28]. As shown in Fig. S2, the EC disinfection efficiency in dark increased at the greater anodic potential values; 9.4, 30, and 82% removal at 1.0, 1.5, and 2 V Ag/AgCl, respectively. The PEC disinfection by far outperformed the EC condition in the same reactor configuration, as previously evinced for aqueous organic pollutants degradation on an analogous self-doped TNT [17]. The external potential directly prompted the charge carrier migration to suppress recombination and to generate surface reactive oxidants under the PEC condition. However, the magnitude of the potential bias showed marginal influence on the PEC disinfection with comparable 3 log inactivation efficiency (for bl-TNT, Fig. S2). This observation justified relatively small anodic bias of 1 V Ag/AgCl employed for the PEC
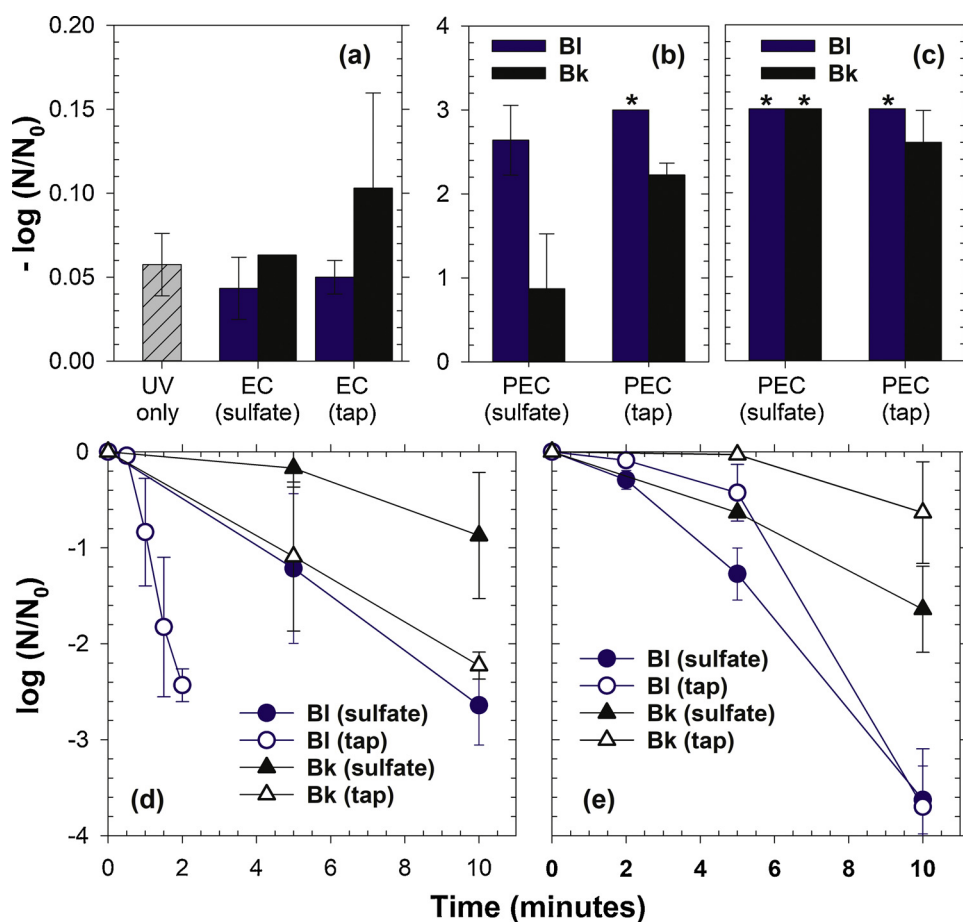
Fig. 4. Photoelectrochemical disinfection activities of bl- and bk-TNT arrays based on logarithmic removal efficiency by (a) PC, EC together with (b) PEC disinfection of *E. coli* and (c) MS2 coliphage during 10 min (* means measurements after 5 min; initial concentration = 10^5 CFU/mL or PFU/mL). The PEC disinfection kinetics at [*E. coli*]$_0$ of (d) 10^5 and (e) 10^7 CFU/mL are also presented (electrolyte = 0.1 M Na$_2$SO$_4$ (sulfate) or tap water; potential bias = 1 V vs. Ag/AgCl).

experiments throughout this study. In addition, both TNT arrays showed negligible visible light responsive activity (data not shown) despite the apparent absorbance (Fig. 2).

It was interesting enough to note significantly invigorated disinfection of *E. coli* on bl-TNT (compared to bk-TNT) and in tap water (compared to Na$_2$SO$_4$ solutions). In contrast, these tendencies of the biocidal efficacy were annihilated for MS2 coliphage; more or less than 3 log removals were obtained within 10 min in all PEC conditions. The bacteria inactivation mostly followed first-order kinetics (Fig. 4d–e) indicating a diffusion controlled reaction [18]. Under [*E. coli*]$_0$ of 10^5 CFU mL^{-1}, the rate constants were in the order of bl (tap) > bl (sulfate) ~ bk (tap) > bk (sulfate) and ca. 2.5-log reduction was possible within 2 min for bl-TNT in tap water. At greater [*E. Coli*]$_0$ of 10^7 CFU mL^{-1}, inactivation in tap water was drastically retarded with initial lag periods.

3.4. Photoelectrochemical degradation of aqueous organic compounds

One would interpret the superior disinfection on the bl-TNT in relation with the generation of reactive oxygen species (ROS) in water as the principal active redox mediator. An oxidation of SO$_4$$^{2-}$ either to S$_2$O$_8$$^{2-}$ or SO$_4$·$^-$ is known to be kinetically limited on TiO$_2$ surface in circum-neutral pH [29]. In order to elucidate the principal oxidant and the overall rate determining step, MB, 4-CP, and RNO were used as model organic compounds with known reactivity with primary ROS species such as ·OH, H$_2$O$_2$, and O$_2$·$^-$ [30]. A notable adsorption of MB (*ca.* 10%) was apparent for bk-TNT in dark (Fig. 5), owing to residual ethylene glycol incompletely oxidized due to annealing in anoxic environment. The dynamic sorption/desorption equilibrium was reached within 20 min for MB, whereas the sorptive removal was negligible for 4-CP and RNO.

Both TNT photoanodes brought about superimposable PEC removal kinetics for the interrogated compounds, in spite of the substantial differences in the bactericidal activities. In 0.1 M Na$_2$SO$_4$ solutions, the degradation rate constant was 1.3 (MB), 9.2 (4-CP), and 4.2 (RNO) h^{-1} for bl-TNT, while 1.5 (MB), 8.4 (4-CP), and 4.4 (RNO) h^{-1} for bk-TNT, respectively. Moreover, the conversion rates in tap water showed marginal differences for MB (1.9 for bl-TNT and 1.5 h^{-1} for bk-TNT) and 4-CP (7.8 for bl-TNT and 6.7 h^{-1} for bk-TNT). Assuming one electron oxidation, a complete transformation of 10 μM organic compounds requires 39 mC (22 μA for 30 min reaction), which rationalized the effective degradation in tap water with minute electrical conductivity. Despite almost complete conversion of MB, the TOC removal efficiency was limited to 29% for bl-TNT and 27% for bk-TNT after 2 h of PEC reactions, which necessitated an extended treatment for a complete mineralization [17]. Oxidation of aqueous pollutants on (photo)electrocatalysts is most often mediated by hydroxyl radicals [2,3] which initiate H-atom abstraction, rapid addition, and direct electron transfer [30]. However, in this study, the pseudo first-order rate constants of substrate degradation were inversely correlated with the bimolecular rate constants with ·OH (2.1 × 10^{10} for MB, 7.6 × 10^9 for 4-CP, and 1.3 × 10^{10} M^{-1} s^{-1} for RNO, respectively [31]). Instead, the rate constants were found to be correlated with the (molecular weight)$^{0.5}$, strongly indicating diffusion controlled reaction. PEC degradation of MB was also examined in the presence of TBA or ME, to quench hydroxyl radicals and/or electron holes. Addition of 0.5 M of scavengers led to incomplete inhibition for both TNTs, with rate constants of 0.90 (TBA) and 0.71 h^{-1} (ME) for bl-TNT, 0.79 (TBA) and 0.87 h^{-1} (ME) for bk-TNT, respectively.
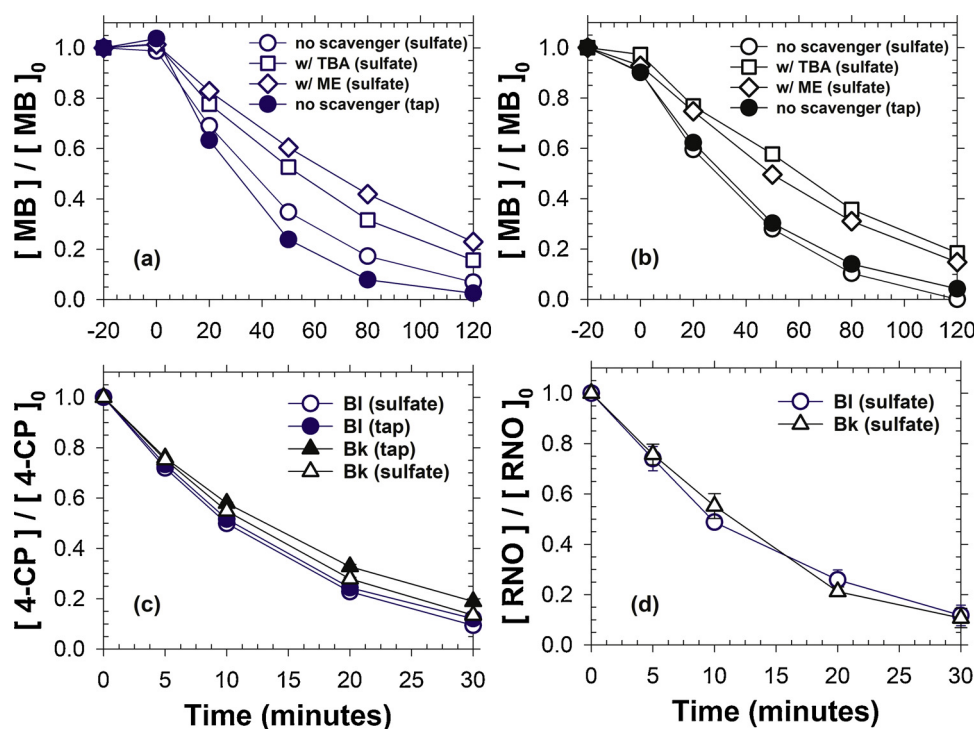
Fig. 5. Photoelectrochemical degradation of organic compounds including (a) MB on bl-TNT, (b) MB on bk-TNT, (c) 4-CP, and (d) RNO ([MB]$_0$ = [4-CP] $_0$ = 10 μM; [RNO] $_0$ = 20 μM; electrolyte: 0.1 M Na$_2$SO$_4$ (sulfate) or tap water; [TBA]$_0$ = [ME]$_0$ = 0.5 M; potential bias = 1 V vs. Ag/AgCl).

3.5. Stability of bl-TNT

Even though the electrochemically reduced TNT arrays was observed to maintain initial color over months in atmosphere, potential re-oxidation of Ti^{3+} under the PEC environment would annihilate the benefits of self-doping. In particular, Ti^{3+} states on surface might be prone to oxidation by atmospheric and aqueous O$_2$ [9]. To our knowledge, an accelerated life time assessment has not been standardized for PEC catalysts, while repetitive disinfection experiments would be time and labor consuming. Thus, the stability of bl-TNT with the superior biocidal activity was assessed in terms of sequential batch degradations of 4-CP. Considering a negligible PEC degradation of 4-CP by intact TNTs without the self-doping (data not shown), physical (detachment of nanotube structure) or chemical (re-oxidation of self-dopants) instability of the bl-TNT would deteriorate the conversion rate.

As shown in Fig. 6a–c, the pseudo first-order rate constant of 4-CP degradation showed marginal variations during the consecutive cycles; the coefficient of variation was far less than 1% in both electrolytes. The used bl-TNT arrays showed bactericidal kinetic constants comparable to the initial value, as shown in Fig. 6d. Judging from the Pourbaix diagram of Ti-H$_2$O system, oxidation of Ti$_2$O$_3$, Ti$_3$O$_5$, and Ti$_4$O$_7$ to TiO$_2$ could occur at an anodic potential lower than 1 V NHE in circumneutral pH [32]. Nevertheless, the rates for 4-CP degradation and disinfection might be independent on the self-dopant density to a certain level under the mass transfer controlled kinetic regime (*vide supra*). The photocurrent from bl-TNT after 70 h continuous operation in Na$_2$SO$_4$ solutions was comparable with the initial value with a moderate fluctuation (Fig. S3). These combined observations suggested that the re-oxidation of Ti^{3+} states would be kinetically limited in our operational condition.

4. Discussion

4.1. Bl- versus Bk-TNT for disinfection

In this study, the crystallinity of TiO$_2$ effectively altered by the annealing temperature (200 versus 450 °C) was suspected to influence not only density [10,13], but also distribution of the self-dopants upon cathodization. The reduction of anatase TiO$_2$ (bl-TNT) would liberate primarily surface dangling oxygen to balance Ti^{3+}, whereas the dopants might propagate into the bulk for bk-TNT arrays to be stabilized during the final annealing (450 °C) in N$_2$ atmosphere [33]. The structural flexibility of amorphous TiO$_2$ would facilitate O$_v$ formation and/or proton intercalation [34], associated with migration of oxide ions and structural distortion (Fig. 2a). Resulting greater donor density in bk-TNT brought about elevated visible light absorption (Fig. 2d), double layer capacitance, and overall photocurrent (Fig. 3a–b), coupled with lower charge transfer resistance (Fig. 3d) [10,17]. The capacitance of TiO$_2$ is known to increase with the doping level owing to the charge trapping/detrapping by mid-gap states [15].

Significantly more efficient PEC disinfection of *E. coli* on bl-TNT (Fig. 4) was, thus, unexpected and initially attributed to a pronounced surface Ti^{3+} for bl-TNT. However, this postulation was rejected by the insignificant Ti^{3+} signal on top surface in XPS (Fig. 2b) which suggested dominant doping on the inner tube wall. The observed greater OER overpotential (Fig. 3) on bl-TNT might suggest weaker surface bonding of OER intermediates (ROS), leading to preferential reactions with substrates [10,35]. The greater bactericidal activities in tap water at [*E. coli*]$_0$ of 10^5 CFU mL^{-1} was also counter-intuitive, especially since [free chlorine] in the absence of microorganisms was always measured to be less than 1 mg L^{-1} during a photo-electrolysis of tap water. An inhibitory effect of sulfate ion on PC disinfection or organics oxidation by TiO$_2$ has been reported previously [29,36], which was ascribed to surface adsorption to block active sites. However, comparable PEC kinetics for organic compounds degradation irrespective of photoanodes and electrolytes (Fig. 5) placed minor importance on the reactivity of surface ROS and the inhibitive surface complexation of
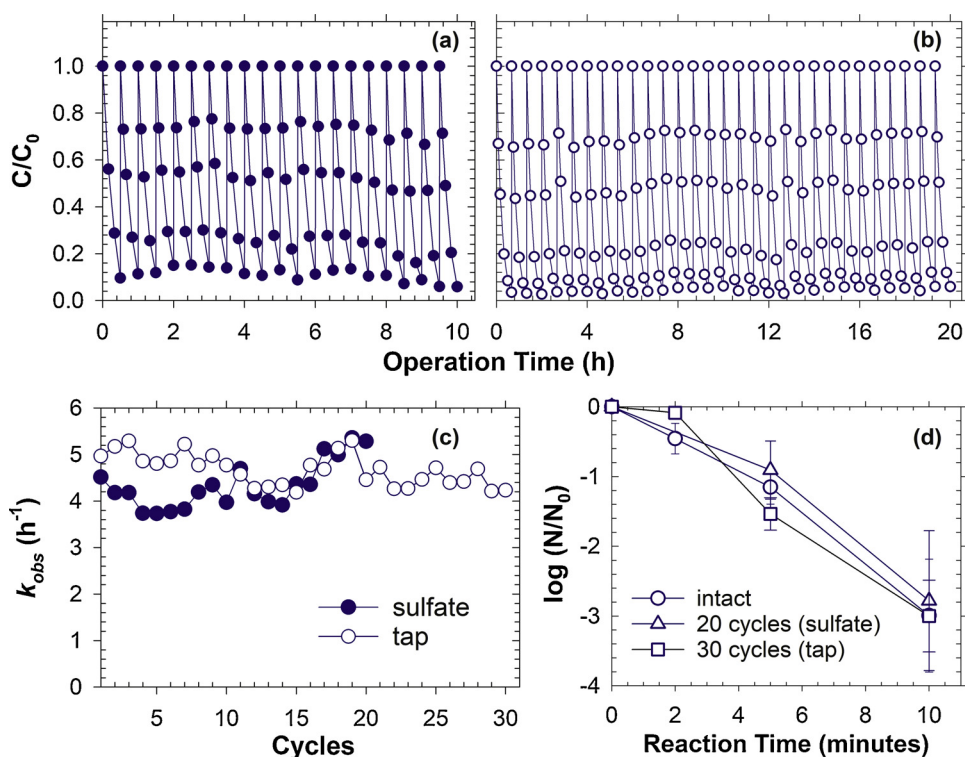
Fig. 6. Long term stability of bl-TNT based on repetitive degradation of 4-CP in (a) sulfate and (b) tap water coupled with (c) variations of pseudo first-order rate constant for 4-CP degradation and (d) PEC disinfection kinetics of *E. coli* before and after the stability experiments ([4-CP]$_0$ = 10 μM; electrolyte = 0.1 M Na$_2$SO$_4$ (sulfate) or tap water; potential = 1 V vs. Ag/AgCl).

SO$_4^{2-}$. A mass transfer controlled regime should be applicable not only for organic compounds degradation but also for disinfection in this study, considering orders of magnitude lower number concentrations of bacterial cells than MB and 4-CP.

In this regard, a deficiency of cations in tap water could permit more negative surface zeta-potential of bacterial cells [37], in-turn augmenting the electrostatic attraction with the photoanode. Disinfection rate constants apparently reduced along with the increase in capacitance further suggested that electrostatic interactions with the electrical double layer (EDL) on photoanode might determine the effective diffusion coefficient and overall disinfection kinetics. In particular, anions (SO$_4^{2-}$) in double layer might decelerate the electrophoretic movements of negatively charged biomass towards the anode surface. The observed capacitance effects (repulsion from co-ions) were less significant for virus cells (Fig. 4c) and neutral organic molecules (Fig. 5). Upon an anodic potential bias, on the other hand, the surface coverage of the dead cells (and debris) *via* capacitive sorption would be more important consideration, along with increasing bio-solids concentration. Assuming spherical morphology with 1 μm diameter, monolayer adsorption of the whole number of *E. coli* cells could cover about 42% of the geometric area at 10^7 CFU mL^{-1} of initial concentration. Evidences of a multi-layer adsorption of bacteria were also presented for porous carbon electrodes at cell voltage of 1.5 V [38]. Thus, a fraction of cell wall surface was assumed to be bound firmly to the double layer with sub-nanometer thickness so that the remaining body would either decrease active surface area or increase tortuosity (diffusion length) of other cells. These speculations on the effects of capacitance were more directly evinced by a potential switching experiment where the adsorbed cells on TNT were repelled by periodic (10 s interval) negative potential (-1 V Ag/AgCl). As illustrated in Fig. 7, inactivation rate of bk-TNT became superimposable with bl-TNT under the switching regime. The surface blocking by captured bacteria was observed to be pronounced in tap water, owing to the tiny concentrations of competing anions, in agreement with the retarded inactivation (with initial lag periods) in tap water at [*E. coli*]$_0$ of 10^7 CFU mL^{-1} (Fig. 4e).
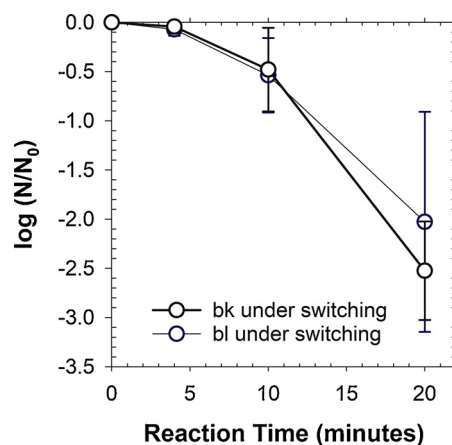

Fig. 7. Effects of potential switching on disinfection ([*E. coli*]$_0$ = 10^7 CFU/mL; electrolyte = 0.1 M Na$_2$SO$_4$; switching potential = ± 1 V vs. Ag/AgCl; switching interval = 10 s).

4.2. Identification of primary oxidants

In this study, ˙OH formation was confirmed by scavenger experiments (Fig. 5a–b) together with the bleaching of RNO (Fig. 5d), an accepted ˙OH probe compound [14]. Nonetheless, the interference of TBA and ME on PEC MB degradation was incomplete, suggesting that a ROS other than ˙OH and electron hole might effectively mediate the organic compounds degradation. Generation of hydrogen peroxide in bulk phase either by water oxidation or O$_2$ reduction was assessed by PEC treatment of 0.1 M Na$_2$SO$_4$ solutions where the accumulated [H$_2$O$_2$] after 1 h was only 35 μM for bl-TNT and 5 μM for bk-TNT. Comparative experiments with added H$_2$O$_2$ stock under UVA irradiation (Fig. S4) demonstrated that 3 log removal within 10 min requires at least 5 mM of H$_2$O$_2$. The negligible variation of photocurrent under a stepwise increase of [MB] at 1 V Ag/AgCl (Fig. S5) also excluded a direct electron transfer from organics to the holes of TNT array. A purging of dissolved oxygen (by bubbling N$_2$ for 0.5 h) prior to the PEC

experiments showed ignorable influence on the conversion of MB (data not shown), rejecting potential formation of superoxide radical anions from the Pt cathode.

In case of the self-doped TNTs, there was a possibility that the hole trapping at surface OH^- and bridging O^{2-} sites [3] might lead to surface peroxo [30] (or active oxygen atom) as a heterogeneous oxidant, by dismutation reactions among bound $\cdot OH$ and lattice $O\cdot^-$ species (similar mechanism to form higher oxide during OER [35]). The O_v in doped TNT might facilitate formation and lattice incorporation of the active O [34], which would be in agreement with the lower OER overpotential for bk-TNT (Fig. 3b) with the elevated donor density. Nevertheless, the ESR spectra of DMPO adducts (Fig. S6) measured after 10 min of PEC reaction were assigned dominantly to OH radical with negligible signal from DMPO-OOH, excluding an effective role of the surface peroxo species. These combined observations ascertained the $\cdot OH$ as the principal oxidant, while the observed imperfect inhibition by TBA and ME would be ascribed to their predominant scavenging of free $\cdot OH$ with rather limited interaction with surface $\cdot OH$ [39] in our experimental conditions.

5. Conclusions

The findings of this study would broaden the applicability of cathodized TNT arrays, by tuning the density and location of self-dopants (Ti^{3+} and O_v), in-turn adjusting the photocurrent, capacitance, OER overpotential, and charge transfer resistance among other properties. For a specific disinfection purpose under diffusion controlled regime, TNT arrays with a lower capacitance (bl-TNT) brought about significantly invigorated bactericidal activity, due to electrostatic interactions between EDL of photoanode and negatively charged bacteria, while the virus disinfection and organic compound degradation were superimposable with analogous bk-TNT array with a greater donor density. The PEC disinfection in tap water, even more effective than in the presence of Na_2SO_4, would allow the bl-TNT to be implemented primarily for point-of-use disinfection in household appliances (*e.g.*, humidifier), to reduce the usage of hazardous chemical reagents such as free chlorine. The experimental conditions of this study would be compatible with commercial 1.5 V battery and UVA LED lamps with relatively low energy loss (heat generation). Rather surprisingly high stability of the bl-TNT for a long-term degradation of organic compound would further strengthen a commercial applicability.

Declaration of interests

The authors declare that they have no known competing financial interests or personal relationships that could have appeared to influence the work reported in this paper.

Acknowledgments

Appendix A. Supplementary data

Supplementary material related to this article can be found, in the online version, at doi:https://doi.org/10.1016/j.apcatb.2019.117910.

References

[1] H. Park, H.I. Kim, G.H. Moon, W. Choi, Photoinduced charge transfer processes in solar photocatalysis based on modified TiO2, Synth. Lect. Energy Environ. Technol. Sci. Soc. 9 (2016) 411–433.

[2] M.R. Hoffmann, S.T. Martin, W.Y. Choi, D.W. Bahnemann, Environmental applications of semiconductor photocatalysis, Chem. Rev. 95 (1995) 69–96.

[3] J. Schneider, M. Matsuoka, M. Takeuchi, J.L. Zhang, Y. Horiuchi, M. Anpo, D.W. Bahnemann, Understanding TiO2 photocatalysis: mechanisms and materials, Chem. Rev. 114 (2014) 9919–9986.

[4] X.B. Chen, L. Liu, F.Q. Huang, Black titanium dioxide (TiO2) nanomaterials, Chem. Soc. Rev. 44 (2015) 1861–1885.

[5] X.B. Chen, L. Liu, P.Y. Yu, S.S. Mao, Increasing solar absorption for photocatalysis with black hydrogenated titanium dioxide nanocrystals, Science 331 (2011) 746–750.

[6] X.B. Chen, L. Liu, Z. Liu, M.A. Marcus, W.C. Wang, N.A. Oyler, M.E. Grass, B.H. Mao, P.A. Glans, P.Y. Yu, J.H. Guo, S.S. Mao, Properties of disorder-engineered black titanium dioxide nanoparticles through hydrogenation, Sci. Rep.-Uk 3 (2013).

[7] T. Berger, T. Lana-Villarreal, D. Monllor-Satoca, R. Gomez, Charge transfer reductive doping of nanostructured TiO2 thin film's as a way to improve their photoelectrocatalytic performance, Electrochem. commun. 8 (2006) 1713–1718.

[8] Y. Yang, M.R. Hoffmann, Synthesis and stabilization of blue-black TiO2 nanotube arrays for electrochemical oxidant generation and wastewater treatment, Environ. Sci. Technol. 50 (2016) 11888–11894.

[9] Z.H. Zhang, M.N. Hedhili, H.B. Zhu, P. Wang, Electrochemical reduction induced self-doping of Ti3 + for efficient water splitting performance on TiO2 based photoelectrodes, Phys. Chem. Chem. Phys. 15 (2013) 15637–15644.

[10] C. Kim, S. Kim, S.P. Hong, J. Lee, J. Yoon, Effect of doping level of colored TiO2 nanotube arrays fabricated by electrochemical self-doping on electrochemical properties, Phys. Chem. Chem. Phys. 18 (2016) 14370–14375.

[11] F. Fabregat-Santiago, E.M. Barea, J. Bisquert, G.K. Mor, K. Shankar, C.A. Grimes, High carrier density and capacitance in TiO2 nanotube arrays induced by electrochemical doping, J. Am. Chem. Soc. 130 (2008) 11312–11316.

[12] N. Liu, C. Schneider, D. Freitag, E.M. Zolnhofer, K. Meyer, P. Schmuki, Noble-metal-Free photocatalytic H-2 generation: active and inactive' black' TiO2 nanotubes and synergistic effects, Chem.-Eur. J. 22 (2016) 13810–13814.

[13] Q. Zheng, H.J. Lee, J. Lee, W. Choi, N.B. Park, C. Leo, Electrochromic titania nanotube arrays for the enhanced photocatalytic degradation of phenol and pharmaceutical compounds, Chem. Eng. J. 249 (2014) 285–292.

[14] C. Kim, S. Kim, J. Lee, J. Kim, J. Yoon, Capacitive and oxidant generating properties of black-colored TiO2 nanotube array fabricated by electrochemical self-doping, Acs Appl. Mater. Inter. 7 (2015) 7486–7491.

[15] H. Zhou, Y.R. Zhang, Electrochemically self-doped TiO2 nanotube arrays for supercapacitors, J. Phys. Chem. C 118 (2014) 5626–5636.

[16] H. Li, Z.H. Chen, C.K. Tsang, Z. Li, X. Ran, C. Lee, B. Nie, L.X. Zheng, T.F. Hung, J. Lu, B.C. Pan, Y.Y. Li, Electrochemical doping of anatase TiO2 in organic electrolytes for high-performance supercapacitors and photocatalysts, J. Mater. Chem. A 2 (2014) 229–236.

[17] M.S. Koo, K. Cho, J. Yoon, W. Choi, Photoelectrochemical degradation of organic compounds coupled with molecular hydrogen generation using electrochromic TiO2 nanotube arrays, Environ. Sci. Technol. 51 (2017) 6590–6598.

[18] P.V.L. Reddy, B. Kavitha, P.A.K. Reddy, K.H. Kim, TiO2-based photocatalytic disinfection of microbes in aqueous media: a review, Environ. Res. 154 (2017) 296–303.

[19] A.E. Mohamed, S. Rohani, Modified TiO2 nanotube arrays (TNTAs): progressive strategies towards visible light responsive photoanode, a review, Energy Environ. Sci. 4 (2011) 1065–1086.

[20] Z.H. Zhang, P. Wang, Optimization of photoelectrochemical water splitting performance on hierarchical TiO2 nanotube arrays, Energy Environ. Sci. 5 (2012) 6506–6512.

[21] Z.H. Zhang, H.J. Wu, Multiple band light trapping in ultraviolet, visible and near infrared regions with TiO2 based photonic materials, Chem. Commun. 50 (2014) 14179–14182.

[22] Z. Li, Y.T. Ding, W.J. Kang, C. Li, D. Lin, X.Y. Wang, Z.W. Chen, M.H. Wu, D.Y. Pan, Reduction mechanism and capacitive properties of highly electrochemically reduced TiO2 nanotube arrays, Electrochim. Acta 161 (2015) 40–47.

[23] J.M. Macak, B.G. Gong, M. Hueppe, P. Schmuki, Filling of TiO2 nanotubes by self-doping and electrodeposition, Adv. Mater. 19 (2007) 3027- + .

[24] F. Zuo, L. Wang, T. Wu, Z.Y. Zhang, D. Borchardt, P.Y. Feng, Self-doped Ti3 + enhanced photocatalyst for hydrogen production under visible light, J. Am. Chem. Soc. 132 (2010) 11856–11857.

[25] C. Di Valentin, G. Pacchioni, A. Selloni, Reduced and n-Type doped TiO2: nature of Ti3 + species, J. Phys. Chem. C 113 (2009) 20543–20552.

[26] S. Trasatti, Electrocatalysis in the anodic evolution of oxygen and chlorine, Electrochim. Acta 29 (1984) 1503–1512.

[27] J. Jeong, J.Y. Kim, M. Cho, W. Choi, J. Yoon, Inactivation of Escherichia coli in the electrochemical disinfection process using a Pt anode, Chemosphere 67 (2007) 652–659.

[28] K. Cho, Y. Qu, D. Kwon, H. Zhang, C.A. Cid, A. Aryanfar, M.R. Hoffmann, Effects of anodic potential and chloride ion on overall reactivity in electrochemical reactors designed for solar-powered wastewater treatment, Environ. Sci. Technol. 48 (2014) 2377–2384.

[29] G.S. Liu, S.J. You, Y. Tan, N.Q. Ren, In situ photochemical activation of sulfate for enhanced degradation of organic pollutants in water, Environ. Sci. Technol. 51 (2017) 2339–2346.

[30] Y. Nosaka, A.Y. Nosaka, Generation and detection of reactive oxygen species in photocatalysis, Chem. Rev. 117 (2017) 11302–11336.

[31] G.V. Buxton, C.L. Greenstock, W.P. Helman, A.B. Ross, Critical-review of rate constants for reactions of hydrated electrons, hydrogen-atoms and hydroxyl radicals

(.Oh/.O-) in aqueous-solution, J. Phys. Chem. Ref. Data 17 (1988) 513–886.

[32] M. Pourbaix, Atlas of Electrochemical Equilibria in Aqueous Solutions, 2d english ed., National Association of Corrosion Engineers, Houston, Tex, 1974.

[33] Y. Yang, L.C. Kao, Y.Y. Liu, K. Sun, H.T. Yu, J.H. Guo, S.Y.H. Liou, M.R. Hoffmann, Cobalt-doped black TiO2 nanotube array as a stable anode for oxygen evolution and electrochemical wastewater treatment, ACS Catal. 8 (2018) 4278–4287.

[34] H.H. Pham, L.W. Wang, Oxygen vacancy and hole conduction in amorphous TiO2, Phys. Chem. Chem. Phys. 17 (2015) 541–550.

[35] C. Comninellis, Electrocatalysis in the electrochemical conversion/combustion of organic pollutants for waste-water treatment, Electrochim. Acta 39 (1994) 1857–1862.

[36] D.M.A. Alrousan, P.S.M. Dunlop, T.A. McMurray, J.A. Byrne, Photocatalytic in-activation of E. Coli in surface water using immobilised nanoparticle TiO2 films, Water Res. 43 (2009) 47–54.

[37] A.T. Poortinga, R. Bos, W. Norde, H.J. Busscher, Electric double layer interactions in bacterial adhesion to surfaces, Surf. Sci. Rep. 47 (2002) 3–32.

[38] D. Golub, E. Benhur, Y. Oren, A. Soffer, Electroadsorption of bacteria on porous carbon and graphite-electrodes, Bioelectrochem. Bioenerg. 17 (1987) 175–182.

[39] M. Cho, H.M. Chung, W.Y. Choi, J.Y. Yoon, Different inactivation behaviors of MS-2 phage and Escherichia coli in TiO2 photocatalytic disinfection, Appl. Environ. Microb. 71 (2005) 270–275.